Journal of Applied Polymer Science

Structure Evolution of Ultra High Molecular Weight Polyethylene/ Montmorillonite Nanocomposite Fibers Prepared by Melt Spinning

Qiang Zhang,[1] Qingzhao Wang,[2] Yong Chen[2]

[1]Analysis and Test Center, School of Materials Science and Engineering, Shandong University of Science and Technology, Qingdao 266590, China

[2]Department of Applied Chemistry, College of Chemical and Environmental Engineering, Shandong University of Science and Technology, Qingdao 266590, China

Correspondence to: Q. Zhang (E-mail: daqiang_1979@163.com)

ABSTRACT: Nanocomposite fibers of ultra high molecular weight polyethylene (UHMWPE) and organic montmorillonite (OMMT) were successfully prepared by a melt-spinning process. The evolution of the microstructures of the nanocomposite fibers in the drawing process was preliminarily studied by X-ray diffraction (XRD), differential scanning calorimetry, and small-angle X-ray scatters. With the increase of draw ratio values, the crystallinity of the nanocomposite fibers increased, the grain size decreased, and the folded chain crystals gradually transformed into extended chain crystals. The results suggested the evolution of the nanocomposite fibers was similar with that of the fibers made by gel-spun drawing process. The addition of OMMT in UHMWPE improved the fluidity of the composites yet without affecting the crystal structure of UHMWPE in the drawing process. © 2013 Wiley Periodicals, Inc. J. Appl. Polym. Sci. 000: 000–000, 2013

KEYWORDS: structure–property relations; X-ray; fibers; differential scanning calorimetry (DSC); crystallization

Received 24 October 2012; accepted 16 June 2013; Published online

DOI: 10.1002/app.39676

INTRODUCTION

The ultra high molecular weight polyethylene (UHMWPE) fiber has attracted great attention due to its low density, solubility properties, and superior mechanical properties including high Young's modulus and tensile strength that are favorable for industrial applications.[1–5] Since the 1970s, UHMWPE fibers have been produced by various drawing methods such as solid state hot drawing,[6,7] solid state extrusion,[8,9] free growth,[10] surface growth,[11] and gel-spinning.[12,13] Among them, one of the most successful methods of commercial introduction of high-strength, high-modulus polyethylene fiber is the process of gel-spinning. This process was discovered and patented in Holland by Dutch State Mines (DSM) and in USA by Allied Signal Corp.[14] At present, the UHMWPE fiber produced by gel-spun has strength of above 3 GPa and is widely used in various areas of industry. But, the apparent disadvantage of the gel-spun method is the use of organic solvents that are difficult to recycle and remove, which results in low productivity, high production costs, and energy consumption.

Melt spinning is an efficient, simple, and nonpolluting method. However, the modulus and strength of melt-spun hot drawn fibers are still much lower than those of gel-spun fiber. This is primarily due to the much lower molecular weight of the polymers used in melt spinning.[15,16] Other disadvantages include the lower level of chain extension and the formation of various types of defects within the fiber.[17–23] The high mechanical properties of the fibers depend on the draw ratio (DR) achieved, but the low molecular weight polymers cannot be super-drawn, while avoiding the large number of defects during drawing. As the unfavorable properties of fibers made by melt spinning are mainly due to the use of the polymers with low molecular weights, high molecular weight polymers like UHMWPE are expected to have much better mechanical properties. However, UHMWPE melts remain in a high elastic state even at close to degradation temperature owning to the random entanglements between the extremely long chains. Therefore, UHMWPE fibers cannot be prepared by melt spinning. UHMWPE needs to be modified to enhance its fluidity and processing performance to use melt spinning method.

In recent years, to improve the processing performance of UHMWPE, much effort has been directed toward modifying UHMWPE to obtain better fluidity. One effective way to reduce the melt viscosity is to dilute the UHMWPE with conventional PE (HDPE, LDPE, and LLDPE), PEG, and PP, etc. that generally have a lower average molecular weight.[24–26] However, this method does not improve the mobility of UHMWPE sufficiently to render it amenable to conventional melt processing. Another effect way is to fill UHWMPE with a small amount of MMT to improve the mobility of the polymer significantly.[27,28]

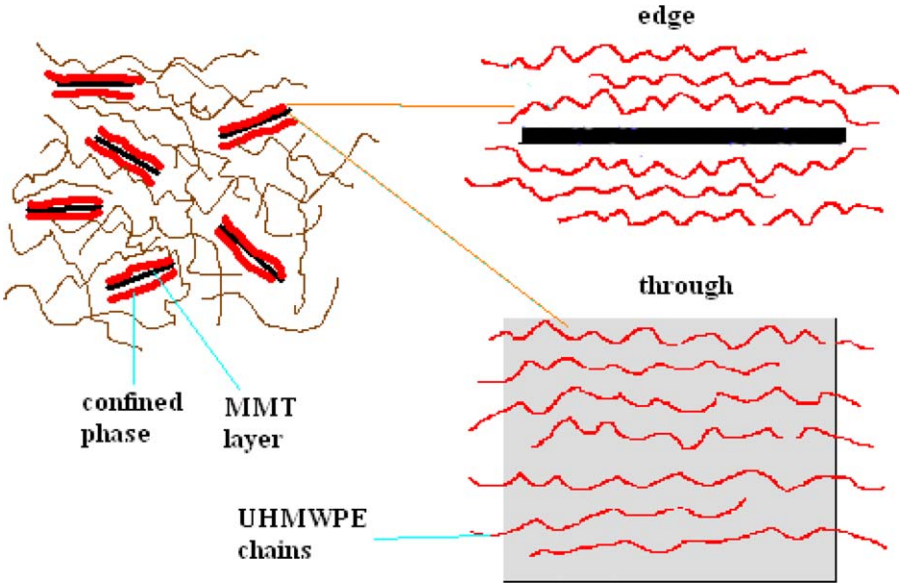

Figure 1. The schematic illustration for dispersed OMMT structure and the structure for confined phase of UHMWPE/OMMT nanocomposites. [Color figure can be viewed in the online issue, which is available at wileyonlinelibrary.com.]

The UHMWPE/organic montmorillonite (OMMT) nanocomposites prepared by means of melt intercalation technique in our laboratory have good fluidity.[29–32] We successfully prepared the UHMWPE/OMMT fiber with the tensile strength of 1.5 GPa by the melt spinning method.[33]

The properties of the fibers depend on its microstructure (grain size, internal defects, the degree of orientation, degree of crystallization, etc.), and the microstructure of the fibers is formed in the drawing process. Structure evolution of UHMWPE fiber in the gel-spun process has been studied by many researchers, and structure evolution of low molecular weight polymer fibers (such as PP, LDPE, and HDPE) in melt spinning process also has been studied by many researchers.[34–38] There have been few studies of structure evolution of the UHMWPE fibers in melt spinning process. In this article, the evolution of microstructures of the UHMWPE fibers during the drawing process was preliminarily studied by XRD, differential scanning calorimetry (DSC), and small-angle X-ray scatters (SAXS). Possible reasons accounting for the improved tensile properties of nanocomposite fibers by melt spinning was proposed.

EXPERIMENTAL

Materials

UHMWPE/OMMT nanocomposite particles: prepared by our laboratory.[31] The molecular weight of UHMWPE is 3×10^6, provided by the Beijing secondary additives Plant; Na-montmorillonite with 200 mesh sizes provided by Shandong laixi bentonite mine and organically modified in our laboratory.[31] The content of Na-based montmorillonite in the UHMWPE/OMMT nanocomposite particles is 5%.

According to our research results, the UHMWPE/OMMT prepared by our laboratory have good fluidly and drawability,[29–32] the MFR of UHMWPE/OMMT nanocomposite particles were 0.5 g/min. As we all know, the pure UHMWPE melts remain high elastic state and low drawability owning to the high molecular chain entanglements degree between the extremely long chains, so we thought that the addition of OMMT decreased of the UHMWPE molecular chain entanglements. Based on our and other groups research, we assumed that the disentanglement mechanism as explained below: OMMT was exfoliated into layers that dispersed in the UHMWPE matrix and the "chemical links"[27] existed between the OMMT layers and the PE molecular chains. The relatively ordered PE chains near the surfaces of the exfoliated OMMT layers formed a lamellar structure named confined phases as schematically depicted in Figure 1. Herein, the term confined phase refers the OMMT and its nearby chains that have different structure and properties from pure UHMWPE. The dispersion of OMMT layers in the UHMWPE is shown on the left of Figure 1. The right upper is the side-view and the right lower is the top-view, respectively. The "chemical links" make the motion of molecular chain in confined phases difficult and lead to a decrease of molecular chain flexibility, so the molecular chains in the confined phases do not entangle with the outside chains and cannot form network structure. Therefore, the molecular chains entanglement density decreased. The decrease of the chain entanglements will improve fluidly and drawability of the UHMWPE.

Preparation of UHMWPE/OMMT Nanocomposite Fibers

Melt spinning was performed on a single-screw melt extruder with a spinneret containing one orifice of 1 mm diameter (L/D =25). The extruder was set with four different temperature zones of 160°C, 190°C, 250°C, and 240°C for Zone 1, Zone 2, Zone 3, and die, respectively. The as-prepared filaments were collected at a take-up speed of 100 m/min and drawn at room temperature with the DR of 1 or 6 on a three-positioned drawing platform, respectively. The as-prepared fiber with the six DR was drawn with DR of 1, 2, 4, 6, 8, and 10 in a hot Silicone oil bath set at 90°C. The total DR of the specimens used in this article was 1, 6, 12, 24, 36, 48, and 60.

Wide-Angle X-ray Diffraction

The wide-angle X-ray diffraction (WAXD) traces were obtained using Rigaku D/Max2500 system utilizing nickel filtered CuK radiation (wavelength of 1.542 Å) and voltage and current settings of 40 kV and 100 mA, respectively; the WAXD data were measured covering a range of 2θ from 16° to 30° with the scanning speed was 2°/min; the WAXD data were measured covering a range of 2θ from 73° to 76° with the scanning speed was 0.2°/min .The two theta angle was calibrated according to the diffraction position of standard Si powder; the peak widths at half-height have been corrected. The apparent crystallite size of a given reflection was calculated using the Scherrer equation:

$$L(hkl) = \frac{K\ \lambda}{\beta \cos\theta} \tag{1}$$

where θ is the Bragg angle for the reflection concerned, λ is the wavelength of radiation (1.542 Å), $L(hkl)$ is the mean length of the crystallite perpendicular to the planes (hkl), β is either the integral breadth or the breadth at half maximum intensity in radians, and K is a Scherrer parameter.

The crystalline chain orientation was evaluated by the Herman orientation function f_c. The WAXD traces were obtained using Rigaku D/Max2500 system with a Rigaku fiber specimen holder. The azimuthal intensity distribution was recorded by step scans at 0.18 intervals in the azimuthal angle. The degree of orientation in the crystalline phases of UHMWPE/OMMT nanocomposite fibers can be obtained through calculation of the Herman orientation function:

$$f_c = \frac{1}{2}\left(3\cos^2\ \varphi\ -1\right) \tag{2}$$

$$\cos^2\ \varphi\ = \frac{\int_0^{\pi/2} I_{hkl} \sin\varphi \cos^2\varphi d\varphi}{\int_0^{\pi/2} I_{hkl} \sin\varphi d\varphi} \tag{3}$$

The f_c takes the value 1 and $-1/2$ with complete orientation parallel and perpendicular to the drawing direction, respectively. The value of $\cos^2\varphi$ in eq. (2) can be calculated from eq. (3), where the azimuthal angle and I_{hkl} is the intensity of a specific (hkl) plane, respectively. The (hkl) plane we used here is the orthorhombic peak (110).

DSC

The DSC experiments were performed using a DSC1 Differential Scanning Calorimeter controlled by a STARe system. Typical sample weights used were ~ 5 mg. A heating rate of 10°C/min and a temperature range from 90°C to 170°C were selected. Indium (m.p. 156.5°C) was used as a calibration standard. The specimens were always tested in a nitrogen environment.

$$X_c = \frac{\Delta H_m}{\Delta H_m^0} \times 100\% \tag{4}$$

where X_c is the degree of crystallinity evaluated by the DSC method, H_m is the melting enthalpy of the sample and H_m^0 is the melting enthalpy of a 100% crystalline sample and is taken as 293 J/g as published in the literature.[39] H_m^0 was corrected by the content of UHMWPE in the composites, which is 95% in the previous work. It is clear that the two-phase model assumes constant amorphous density in highly oriented samples while disregarding the presence of an oriented intermediate phase.

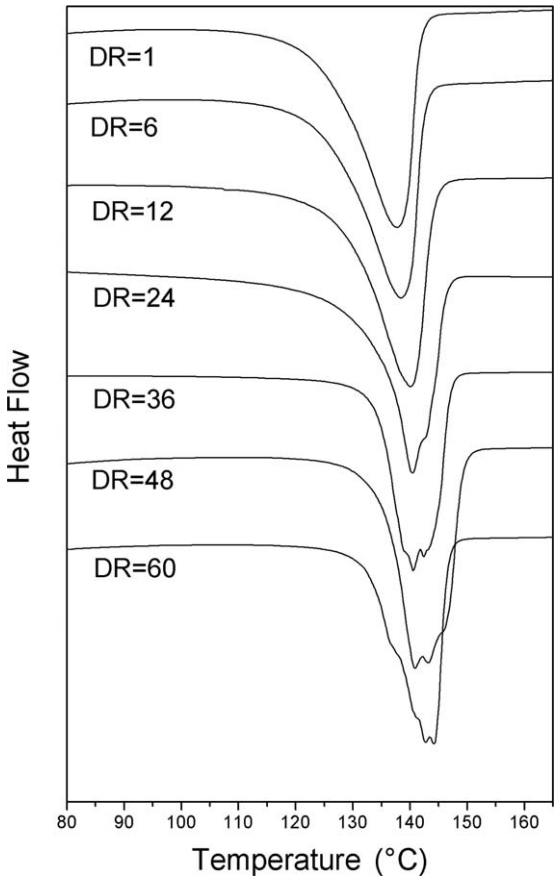

Figure 2. DSC thermograms of as-prepared and drawn UHMWPE/OMMT fiber specimens with different DR values.

SAXS

SAXS experiments were performed using the BL16B1-SAXS of Shanghai Synchrotron Radiation Facility with Electron energy of 3.5 GeV and wavelength of 1.240 Å, the sample-to-detector distance was 5200 mm. The two-dimensional scatter data was integrated with FIT2D software integration, and the SAXS two-dimensional image was converted into one-dimensional data.

RESULTS AND DISCUSSION

DSC Data Analysis

Figure 2 shows the DSC thermograms of as-prepared and drawn UHMWPE/OMMT fiber specimens with different DR values. As can be seen in Figure 2, DSC curves of as-prepared specimen and specimens with DR values lower than 12 only contained one melting endotherm peak and their shape did not vary significantly as DR values increase from 1 to 12. The peak melting temperature increased from 137.1°C to 139.5°C as DR values increase from 1 to 12, indicating that the crystal structure

Applied Polymer SCIENCE

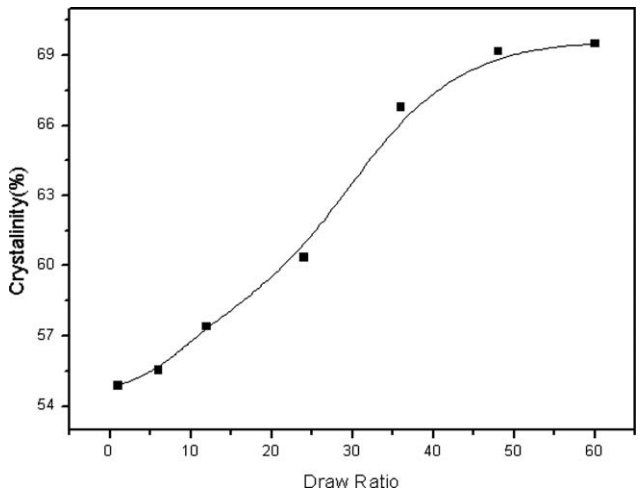

Figure 3. The crystallinity values of as-prepared and drawn UHMWPE/OMMT composite fiber specimens with varying DR values.

of as-prepared and drawn UHMWPE/OMMT fiber specimens with DR values less than 12 did not change obviously. The crystalline phase exhibited a folded chain structure in these cases. This stage of drawing process aims to make the folded chains perfect and only a very few amorphous phases transform into crystalline phases. A shoulder occurred at the right side of the main melting peak of the nanocomposite fiber that was drawn to 24 ratios. The shoulder became a melting peak of a value of $\sim$ 142°C when the nanocomposite fiber was drawn to 36 ratios. The endotherm peak at $\sim$ 142°C is originated from the melting of the extended chain crystals,[40] suggesting that folded chains gradually transform into extended chain crystals. In addition, the second melting peak became stronger with the increase of DR, indicating that the content of extended chain crystals kept increasing. When drawn to 60 ratios, the second melting peak was stronger than the first melting peak that indicates the content of extended chains is higher than that of the folded ones in the nanocomposite fibers. Thus, further drawing of nanocomposite fibers is reasonable expected to eliminate folded chain crystals and improve tensile strength.

Figure 3 presents DSC analysis data. As can be seen in Figure 3, the DSC crystallinity increased from 54% to 57% gradually as DR values increase from 1 to 12. According to the research reports on gel spinning fibers, the DSC crystallinity decreases in the process of gel spinning during the initial drawing process.[41,42] This initial decrease of crystallinity did not occur in our experimental system possibly because the drawing temperature (90°C) was significantly lower than the melting temperature of as-prepared fibers. Moreover, at this stage, the structure of the crystalline region and amorphous region in the as-prepared fibers was relatively loose, and the tensile stress was relatively small, so the degree of crystallinity increased gradually. DSC crystallinity goes up from 57% to 66% rapidly as DR values increase from12 to 36, possibly due to partial molecules in the amorphous area were slightly intertwined with other molecules and were straightened, thereby forming a new crystalline region. Moreover, the molecular chains in the defective crystalline area were drawn and then gradually participated in the crystals of straightened chains. Therefore, DSC crystallinity increased rapidly, whereas defects declined quickly, as shown in the SAXS data presented below. DSC crystallinity increased from 66% to 69% slightly as DR values increase from 36 to 60 possibly because the nanocomposite fibers were highly dense and contained minimal defects. The SAXS data indicated that the degree of defects does not change after the fibers were drawn to 36 ratios or above.

X-Ray Diffraction Data Analysis

Orthorhombic crystals are the stable crystal type of polyethylene, whose X-ray diffraction curve contains two typical characterized peaks, namely, the diffraction peaks of the (110) and (200) crystal planes. Moreover, the 2θ of peak positions are 21.5° and 24°, respectively. As can be seen in Figure 4, all the sample fibers contained characterized diffraction peaks of (110) and (200) crystal planes at $2\theta = 21.4°$ and 24°, respectively. The intensity and FWHM increased gradually with increasing DR values. Notably, the sample that was drawn 60 ratios presented a relatively small diffraction peak[43–45] corresponding to the monoclinic (001) plane at $2\theta = 19.6°$. These features were also observed in the results of the gel system, which demonstrated that OMMT does not have influence on crystal variation during the drawing process.

Figure 5 shows X-ray diffraction analysis results for (110) plane, (200), and (002) plane, The 2θ breadth of the 002 reflection of these samples provides a measure of the crystal size in the direction of the chain axis. The size of the crystal corresponding to each crystal plane was the mean value calculated using the Scherer formula. As can be seen in Figure 5, as their DR values

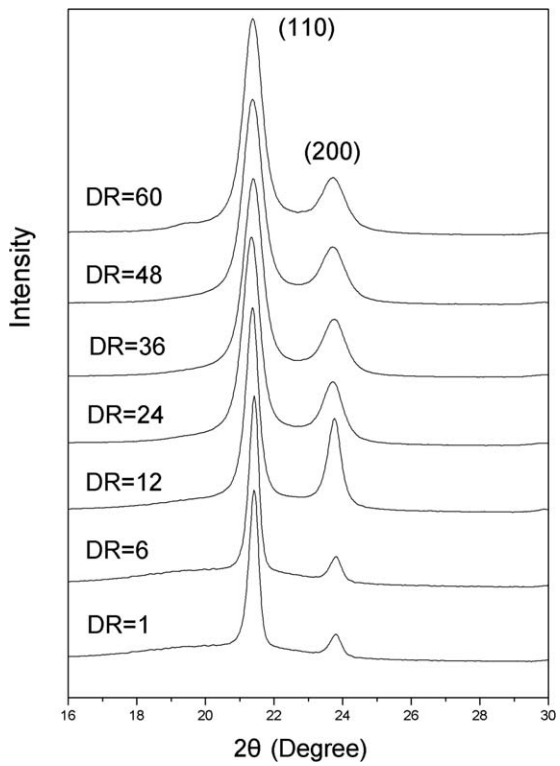

Figure 4. WAXD patterns of as-prepared and drawn UHMWPE/OMMT fiber specimens with different DR values.

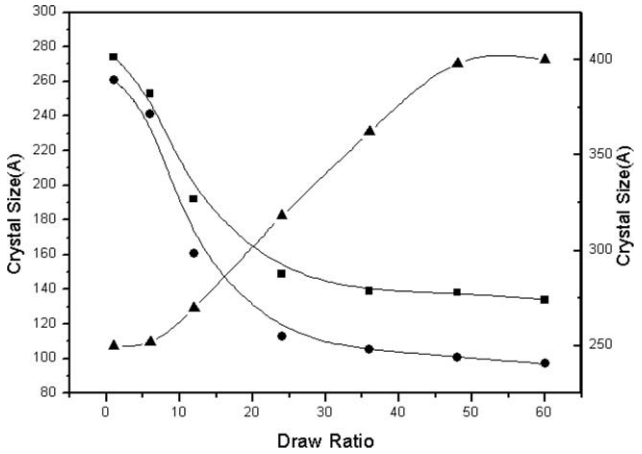

Figure 5. The crystal size (■:110 plane●:200 plane▲:002 plane) of as-prepared and drawn UHMWPE/OMMT composite fiber specimens with varying DR values.

increased from 1 to 36, the mean size of the crystals in the normal direction of (110) plane and (200) plane decreased rapidly with increasing drawn ratios and the dropping trend gradually decreased. As the DR values increased from 36 to 60, crystallite sizes of (110) plane and (200) plane remained at a balanced value 130 Å and 100 Å. At the same time, as their DR values increased from 1 to 36, the longitudinal crystallite size of (002) plane increased rapidly. As the DR values increased from 36 to 60, the longitudinal crystallite size of (002) plane remained at a balanced value 380 Å. Variations in crystallite size can be attributed to the following two aspects: crystals that are vertical to the drawing direction lean along the drawing direction and fibrillar tight molecules were torn at the defective place in the initial drawing process; and the crystals compact and perfect themselves during drawing process. Therefore, the apparent crystal size of (110) plane and (200) plane decreased, and the crystal size of (002) plane in the direction of the chain axis increased. Eventually, the crystallite sizes did not change further. Previous studies[46] reported that MMT can play the role of heterogeneous nucleation in a composite material because of its

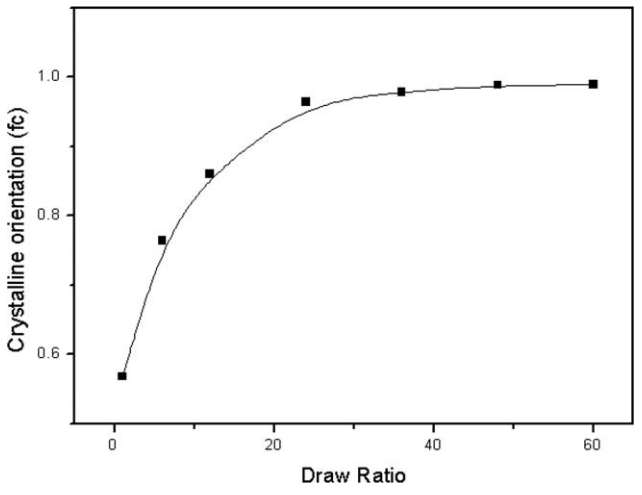

Figure 6. The crystal orientation of as-prepared and drawn UHMWPE/OMMT fiber specimens with different DR values.

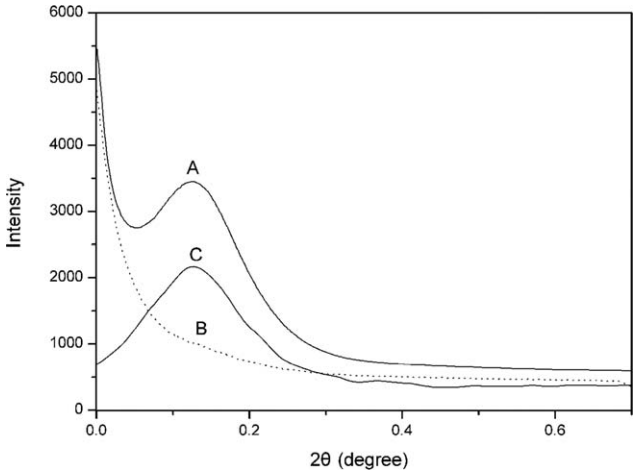

Figure 7. Correction of the SAXS patterns intensity curves of a UHMWPE/OMMT fiber (A-observed SAXS curve of the sample, B-background curve, C-corrected SAXS intensity curve of the sample).

nucleation and growth mechanisms, differing from that of polyethylene. Under the same conditions, composite materials enjoyed a higher crystallization rate, which resulted in a bigger crystallite size. Based on our obtained data, the crystallite size of the nanocomposite fibers that was 60 DR was similar with that observed in the fibers made by gel spinning.[41] MMT did not influence the change in crystallite size during the drawing process.

Figure 6 shows the crystalline orientation (f_c) values of as-prepared and drawn UHMWPE/OMMT fiber specimens with different DR values. f_c values were found through calculation of the Herman orientation function of the (110) plane of the orthorhombic crystals present in drawn UHMWPE fiber specimens. As can be seen in Figure 6, the f_c values of the drawn UHMWPE fibers increased rapidly from 0.57 to 0.96 as the DR values increased from 1 to 24. The f_c values increased from 0.96 to 0.98 as the DR values increased from 24 to 48. The increasing rates of f_c values decreased significantly, when the DR values of the drawn UHMWPE/OMMT fibers increased from 48 to 60, and the f_c values of the drawn UHMWPE fibers initially increase from 0.98 to 0.99, showing nearly perfect chain orientation. Based on our obtained data, the crystalline orientation (f_c) values of as-prepared and drawn UHMWPE/OMMT fiber specimens with different DR values was similar with that observed in the fibers made by gel spinning.[47]

SAXS Data Analysis

The SAXS pattern originates from defects and long-range ordered structure in the fiber specimen,[48] in which the defects include the two parts of crystalline defects and noncrystalline defects. In SAXS pattern, the higher the degree of fiber defects, the greater the SAXS scattering intensity.

The SAXS data was processed to get quantitative results. The processing procedure was shown in Figure 7. Curve A was the scattering curve directly obtained by the instrument. The dotted line B was the scattering curve of the X-ray against a blank background, that is, no sample was involved (attenuation curve). Deducting the factors of Curve B from Curve A

produced Curve C, which was the true SAXS scattering curve of the sample. Curve C displayed a scattering peak position and scattering intensity. Except for the internal structural factors, the absolute value of the scattering intensity is related to sample quantity and instrument status. This study measured SAXS by using the same instrument status and the same quantity samples with different structures. We calibrated and calculated the unit weight intensity, which is recorded as the SAXS intensity. Figure 8 shows SAXS scattering intensity of as-prepared and drawn UHMWPE/OMMT fiber specimens with different DR values. The scattering intensity of SAXS patterns of UHMWPE/OMMT fibers decreases with the increase of DR. SAXS scattering intensity decreased rapidly as DR values increased from 1 to 24 and decreased gradually as DR values increased from 24 to 60. This result may be due to the fact that the as-prepared fiber contains a lot of loose amorphous phase as mentioned in DSC analysis. At this stage of drawing, the polyethylene macromolecular chains slipped rapidly as their DR values increased from 1 to 24, and the loose amorphous phase was easily stretched to produce a certain orientation. Therefore, we hypothesize that as defects decrease rapidly, a part of taut tie molecules connecting the lamellae crystals were straightened, and folded chain lamellae connected with the taut tie molecules unfolded to form a new crystal region. At the second stage of drawing (24 to 60), the fiber structures became more compact and the crystals contained fewer defects, thus the degree of defects did not change very much.

The crystal long period was calculated by Bragg equation, Figure 9 shows the crystal long period of as-prepared and drawn UHMWPE/OMMT fiber specimens with different DR values. As can be seen in Figure 9, the crystal long period size increased gradually as DR values increased from 1 to 6; the crystal long period size increased rapidly as DR values increased from 6 to 48; as DR values increased from 48 to 60, the crystal long period size remained at a balanced value, about 800 Å. According to the research reports on gel spinning fibers, the crystal long period size of the gel-spun UHMWPE fiber remained 1500–2000 Å,[49] the lower crystal long period size may be the key restrictions in the further improvement of the mechanical properties of the melt spun UHMWPE/OMMT fiber.

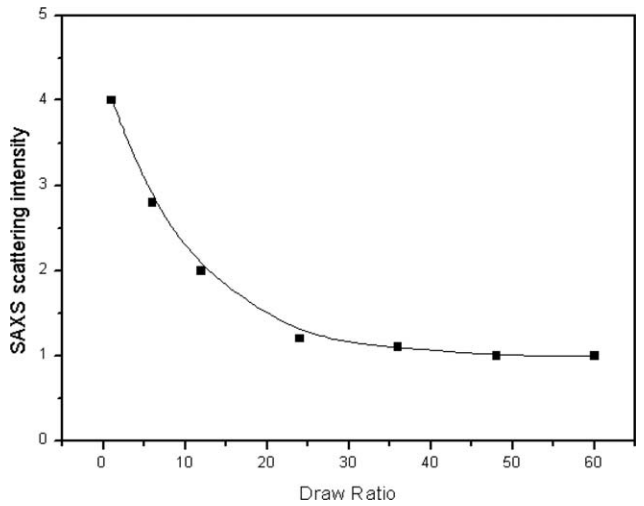

Figure 8. SAXS scattering intensity of as-prepared and drawn UHMWPE/OMMT fiber specimens with different DR values.

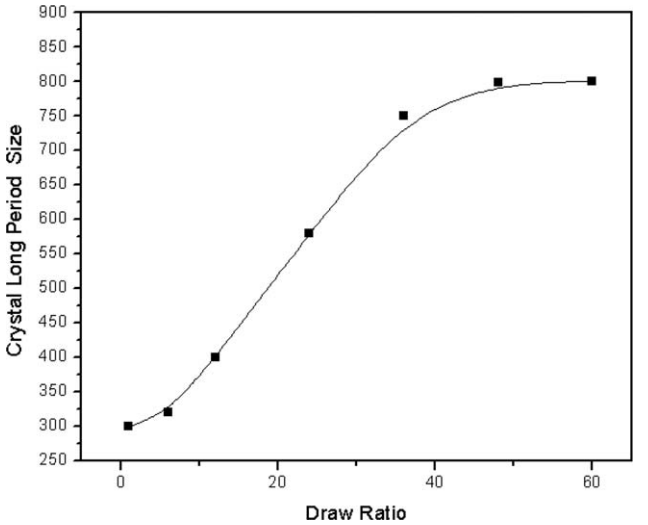

Figure 9. The crystal long period size of as-prepared and drawn UHMWPE/OMMT fiber specimens with different DR values.

CONCLUSIONS

The evolution of microstructures of the UHMWPE/OMMT nanocomposite fibers during the drawing process were preliminarily studied by XRD, DSC, and SAXS. The crystallinity of the specimens increased from 54% to 57% gradually as DR values increased from 1 to 12 and rapidly went up from 57% to 66% as DR values increased from 12 to 36. The crystallinity slightly increased from 66% to 69% as DR values increased from 36 to 60. The size of the crystals in the normal direction of (110) plane and (200) plane decreased rapidly as DR values increased from 1 to 36 and remained at a constant value as DR values increased from 36 to 60; The size of the crystals in the drawn direction of (002) plane increased rapidly as DR values increased from 1 to 36 and remained at a constant value 380 Å as DR values increased from 36 to 60. The degree of defects of the specimens decreased rapidly as DR values increased from 1 to 24 and decreased slightly as DR values increased from 24 to 60. The f_c values of the specimens increased rapidly from 0.57 to 0.96 as the DR values increased from 1 to 24. The f_c values increased from 0.96 to 0.98 as the DR values increased from 24 to 48. The f_c values increased from 0.98 to 0.99 as the DR values increased from 48 to 60, showing nearly perfect chain orientation. The crystal long period size remained 800 Å and far lower than that of the gel-spun UHMWPE fiber. With the increase of DR values, folded chain crystals gradually transform into extended chain crystals and the content of extended chain crystals is higher than that of the folded ones in the fibers that were drawn to 60 ratios. The evolution of microstructures of the UHMWPE fibers made by melt spinning was similar with that of the fibers made by gel-spun in drawing process. The OMMT did not affect the change trend of crystal structure of the specimens in the drawing process.

REFERENCES

1. Smith, P.; Lemstra, P. *J. Macromol. Chem.* **1979**, *180*, 2983.
2. Pan, W.; Liu, Z.-F.; Hu, Z.-M.; Chen, L.; Zhu, J.; Yu, Y.-R. *SFC* **2006**, *11*, 6.
3. Ward, I. M.*Macromol. Symp.* **1995**, *100*, 1.
4. Li, Q.; Yang, G.; Li, Y.; Lu, W.; Ye, Z. *Chin. J. Colloid Polym.* **2009**, *27*, 30.
5. You, X.; Hu, P.; Liu, Z. *J. Text. Res.* **2010**, *31*, 146.
6. Andrews, J. M.; Ward, I. M. *J. Mater. Sci.* **1970**, *5*, 411.
7. Capaccio, G.; Ward, I. M. *Polymer* **1975**, *16*, 239.
8. Perkins, W. M.; Capiati, N. J.; Porter, R. S. *Polym. Eng. Sci.* **1976**, *16*, 200.
9. Kanamoto, T.; Tsuruta, A.; Tanaka, K.; Takeda, M.; Porter, R. S. *Macromolecules* **1988**, *21*, 470.
10. Zwijnenburg, A.; Pennings, A. *J. Colloid Polym. Sci.* **1975**, *253*, 452.
11. Zwijnenburg, A.; Pennings, A. J. *J. Polym. Sci. Polym. Lett. Ed.* **1976**, *14*, 339.
12. Smith, P.; Lemstra, P. J. *J. Mater. Sci.* **1980**, *15*, 505.
13. Kavesh, S.; Prevorsek, D. C. U.S. *Pat. 4*,413,110 (**1983**).
14. Smith, P.; Lemstra, P. J. U.K. *Pat. 2*,040,414 (**1979**).
15. Smith, P.; Lemstra, P. J.; Pijpers, J. P. L. *J. Polym. Sci. Polym. Phys. Ed.* **1982**, *20*, 2229.
16. Hallam, M. A.; Pollard, G.; Ward, I. M. *J. Mater. Sci. Lett.* **1987**, *6*, 975.
17. Zhurkov, S. N.; Zakrevskyi, V. A.; Korsukov, V. E.; Kuksenko, V. S. *J. Polym. Sci. Part A-2: Polym. Phys.* **1972**, *10*, 1509.
18. Kuksenko, V. S.; Ryskin, V. S.; Betekhtin, V. I.; Slutsker, A. I. *Int. J. Fract.* **1975**, *11*, 829.
19. Jarecki, L.; Meier, D. J. *J. Polym. Sci. Polym. Phys. Ed.* **1979**, *17*, 1611.
20. Wu, W.; Black, W. B. *Polym. Eng. Sci.* **1979**, *19*, 1163.
21. Amornsakchai, T.; Cansfield, D. L. M.; Jawad, S. A.; Pollard, G.; Ward, I. M. *J. Mater. Sci.* **1993**, *28*, 1689.
22. Amornsakchai, T.; Olley, R. H.; Bassett, D. C.; Al-Hussein, M. O. M.; Unwin, A. P.; Ward, I. M. *Polymer* **2000**, *41*, 8291.
23. Amornsakchai, T.; Songtipya, P. *Polymer* **2002**, *43*, 4231.
24. Dumoulin, M. M.; Utracki, L. A.; Lara, *J. Polym. Eng. Sci.* **1984**, *24*, 117.
25. Kyu, T.; Vadhar, P. *J. Appl. Polym. Sci.* **1986**, *32*, 5575.
26. Xie, M. J.; Liu, X. L.; Li, H. L. *J. Appl. Polym. Sci.* **2006**, *100*, 1282.
27. Wu, Q. Y.; Gao, W. P.; Hu, Y. L. *J. Appl. Polym. Sci.* **2001**, *80*, 2154.
28. Gai, J.; Li, H. *J. Appl. Polym. Sci.* **2007**, *106*, 3023.
29. Wang, Q.; Liao, X., Liu, Z. *J. Chem. Res. Chin. Univ.* **2004**, *4*, 504.
30. Wang, Q.; Liu, Z. *J. China Plast.* **2004**, *5*, 32.
31. Wang, Q.; Liu, Z. *J. China Plast.* **2003**, *8*, 32.
32. Wang, Q.; Liu, Z. *J. Eng. Plast. Appl.* **2003**, *10*, 46.
33. Zhen, W.; Wang, Q.; Wu, J.; Wang, H. *J. Synth. Fiber China* **2011**, *3*, 5.
34. Rangasamy, L.; Shim, E.; Pourdeyhimi, B. *J. Appl. Polym. Sci.* **2011**, *120*, 410.
35. Lee, S. H.; Youn, J. R. *J. Appl. Polym. Sci.* **2008**, *109*, 1221.
36. Zhang, X.; Yang, M.; Zhao, Y.; Zhang, S.; Dong, X.; Liu, X.; Wang, D.; Xu, D. *J. Appl. Polym. Sci.* **2004**, *92*, 552.
37. Hao, C.; Zhao, Y.; He, A.; Zhang, X.; Wang, D.; Ma, Q.; Xu, Y. *J. Appl. Polym. Sci.* **2010**, *116*, 1384.
38. Chantrasakul, S.; *Amornsakchai, T.* DOI 10.1002/pen.20778.
39. Wunderlich, B.*Macromol. Phys.* **1980**, *3*, 69.
40. Smook, J.; Pennings, J. *J. Colloid Polym. Sci.* **1984**, *262*, 712.
41. Karacan, I. *J. Appl. Polym. Sci.* **2006**, *101*, 1317.
42. Liu, L.; Zhu, X.; Deng, T.; Zhang, G.; Fang, L. *Mater. Sci. Technol.* **2005**, *13*, 489.
43. Pennings, J.; Zwijnenburg, A. *Polym. Sci. Polym. Phys. Ed.* **1979**, *17*, 1011.
44. Kwon Y. K.; Boller A.; Pyda M.; Wunderlich B. *Polymer* **2000**, *41*, 6237.
45. Tashiro, K.; Sasaki, S.; Kobayashi, M. *Macromolecules* **1996**, *29*, 7460.
46. Liu, Z.; Hu, Z.; Chen, Z. *J. China Text. Univ.* **1992**, *1*, 41.
47. Yeh, J.-T.; Lin, S.-C.; Tu, C.-W.; Hsie, K.-H.; Chang, F.-C. *J. Mater. Sci.* **2008**, *43*, 4892.
48. Ohta, T.*Polym. Eng. Sci.* **1989**, *23*, 697.
49. Grubb, D. T.; Prasad, K. *Macromolecules* **1992**, *25*, 4575.